Communication

Photonic Bandgap Closure and Metamaterial Behavior in 1D Periodic Chains of High-Index Nanobricks

Evelyn Díaz-Escobar [1], Laura Mercadé [1,2], Ángela I. Barreda [3], Jaime García-Rupérez [1] and Alejandro Martínez [1,*]

1   Nanophotonics Technology Center, Universitat Politècnica de València, Camino de Vera s/n, 46022 Valencia, Spain
2   MIND-IN2UB, Departament d'Electrònica, Facultat de Física, Universitat de Barcelona, Martí i Franquès 1, 08028 Barcelona, Spain
3   Institute of Applied Physics, Abbe Center of Photonics, Friedrich Schiller University Jena, Albert-Einstein-Str. 15, 07745 Jena, Germany
*   Correspondence: amartinez@ntc.upv.es

Abstract: It has been shown that the photonic bandgap of one-dimensional (1D) dielectric periodic thin films can vanish at the first Bragg condition for TM modes. Here, we address the case of 1D photonic crystal slabs formed by a chain of high-index dielectric particles with transversal confinement and show that the Bragg bandgap can vanish for both TE- and TM-like modes. Calculations using plane-wave expansion and finite-difference time-domain methods confirm that the PBG vanishes. PBG closure is explained as being a result of the interplay between the electric and magnetic dipole resonances of the isolated nanoparticle with Bragg resonance, as confirmed by calculating the electric and magnetic dipoles of the isolated nanobricks. This can be considered as a manifestation of the metamaterial behavior of the 1D system when using silicon as an underlying material. Our finding may have important consequences for the fields of photonic crystals and all-dielectric metamaterials.

Keywords: photonic bandgap; 1D periodic chains; silicon photonics; metamaterials; Mie resonances

1. Introduction

The periodic modulation (period a) of the index of refraction of a dielectric medium gives rise to photonic band gaps (PBGs) where electromagnetic propagation along the direction of periodicity is forbidden [1]. If we consider a periodic medium formed by periodic layers of indices n_1 and n_2, a so-called 1D photonic crystal, the lowest-frequency PBG opens due to the splitting of the so-called dielectric and air bands at the Bragg wavelength, defined as $\lambda = 2\overline{n}a$, where $\overline{n} \approx \frac{n_1+n_2}{2}$. Interestingly, the width of the PBG is directly proportional to the index contrast, as $\Delta n \approx \frac{n_1-n_2}{\overline{n}}$. This essentially means that the PBG arises even for minute values of Δn, as in the case of fiber Bragg gratings used as wavelength filters in telecom networks [2], and can become very large when high-index materials—such as silicon—are used. Indeed, the existence of full, three-dimensional (3D) PBGs in 3D photonic crystals can be explained as the overlapping of wide 1D-PBGs in every possible spatial direction, i.e., for every possible wave vector k [3,4].

The first PBG is remarkably important in integrated guided optics since it is usually the only one placed below the light cone [5,6]; therefore, it can give rise to localized modes with large Q factor when defect-like cavities are created. In the integrated optics arena, the confinement of light waves below the light line is achieved due to total internal reflection in the two dimensions perpendicular to the propagation direction, in which the system is periodic.

Recently, it has been shown theoretically [7] that the first (or Bragg) PBG can vanish in a 1D periodic thin film, though only for TM modes (with the electric field perpendicular to the film) and not for TE modes (with the electric field parallel to the film). This result

is explained from the different boundary conditions to be satisfied by the electric and magnetic fields when propagating along the periodic film. However, this study was two-dimensional (2D) and did not include lateral confinement of the waves. From a practical perspective, it would be interesting to see whether the closure of the PBG is also maintained when transversal confinement via total internal reflection (TIR) is introduced, as in 1D photonic crystal slabs [8] built in high-index films.

Here, we study a 1D photonic crystal with full transversal confinement formed by a set of silicon nanobricks and show that the Bragg PBG for TE-like modes can vanish under proper conditions. We choose this system because it allows for an easy analysis of the unit cell and can be easily fabricated using standard silicon micro- and nanofabrication tools, as shown in recent experiments [9–11]. Notably, interchanging the thickness and the width of the nanobricks should also lead to the closure of the PBG for TM-like modes, in contrast to the case addressed in [7]. To explain the closure, and since we cannot describe the system analytically, we adopt a strategy different to [7] and consider the electric and magnetic Mie resonances of the isolated nanobricks. Our results suggest that the interplay between both Mie resonances and the Bragg resonance leads to PBG closure, resulting in a metamaterial-like behavior of the periodic structure.

2. Results

We consider a periodic structure made of high-index (n = 3.5) nanobricks with the dimensions of w_x, w_y and w_z surrounded by air (see Figure 1a). The structure is periodic along the z axis (period a), whilst confinement of guided waves in the x and y direction is ensured by TIR. Figure 1b shows the photonic bands—calculated using the plane wave expansion method—of the TE-like (or x-even parity) modes for w_x = 220 nm, w_y = 450 nm, and a = 455 nm for three different values of w_z. Notice that, due to the addition of the confinement along the y direction, we cannot classify the guided modes into TE or TM since the three components of the electric and magnetic fields are now present [12]. Nonetheless, the modes are usually termed either TE-like (the main component of transverse field is E_y) or TM-like (the main component of transverse field is E_x) in integrated optics due to their resemblance to the 2D picture. When w_z = 200 nm (blue curves), a wide TE PBG opens between the dielectric and the air bands, as expected for high-contrast periodic systems [1]. The same happens for w_z = 320 nm (red curves), though the PBG is redshifted because of the larger amount of dielectric material in the unit cell.

When, analyzing the intermediate case (w_z = 260 nm, black curves) we observe that the PBG vanishes. This means that the PBG width is neither directly nor inversely proportional to the parameter w_z. To know more about this relation, we calculate the frequencies of the dielectric and air bands at the boundary of the first Brillouin zone. Notice that these frequencies establish the boundaries of the Bragg bandgap. The results, depicted in Figure 1c, clearly show a crossing of the bands—or band flip [7]—delimiting the Bragg PBG at $w_z \approx 258$ nm. This means that, counterintuitively, the PBG vanishes even though we have a high-index contrast system. In general, an increase in w_z results not only in a red-shift of the bands but also in a modification of the width of the Bragg PBG that eventually closes. To establish the effect of the period on PBG closure, we performed calculations for other values of a. We observed that the PBG was effectively closed at w_z = 248 nm for a = 430 nm and at w_z = 267 nm for a = 480 nm, meaning that the effect was also observed for other periods of the lattice.

In comparison to the results in [7], we may argue that we now have TIR confinement in the lateral direction, which resembles the TE case found there. Indeed, by interchanging w_x and w_y in our periodic system (or rotating the structure 90° around the z axis), we should find that the PBG closes for TM-like (or x-odd parity) modes, meaning that the first PBG can be closed irrespective of the type of mode.
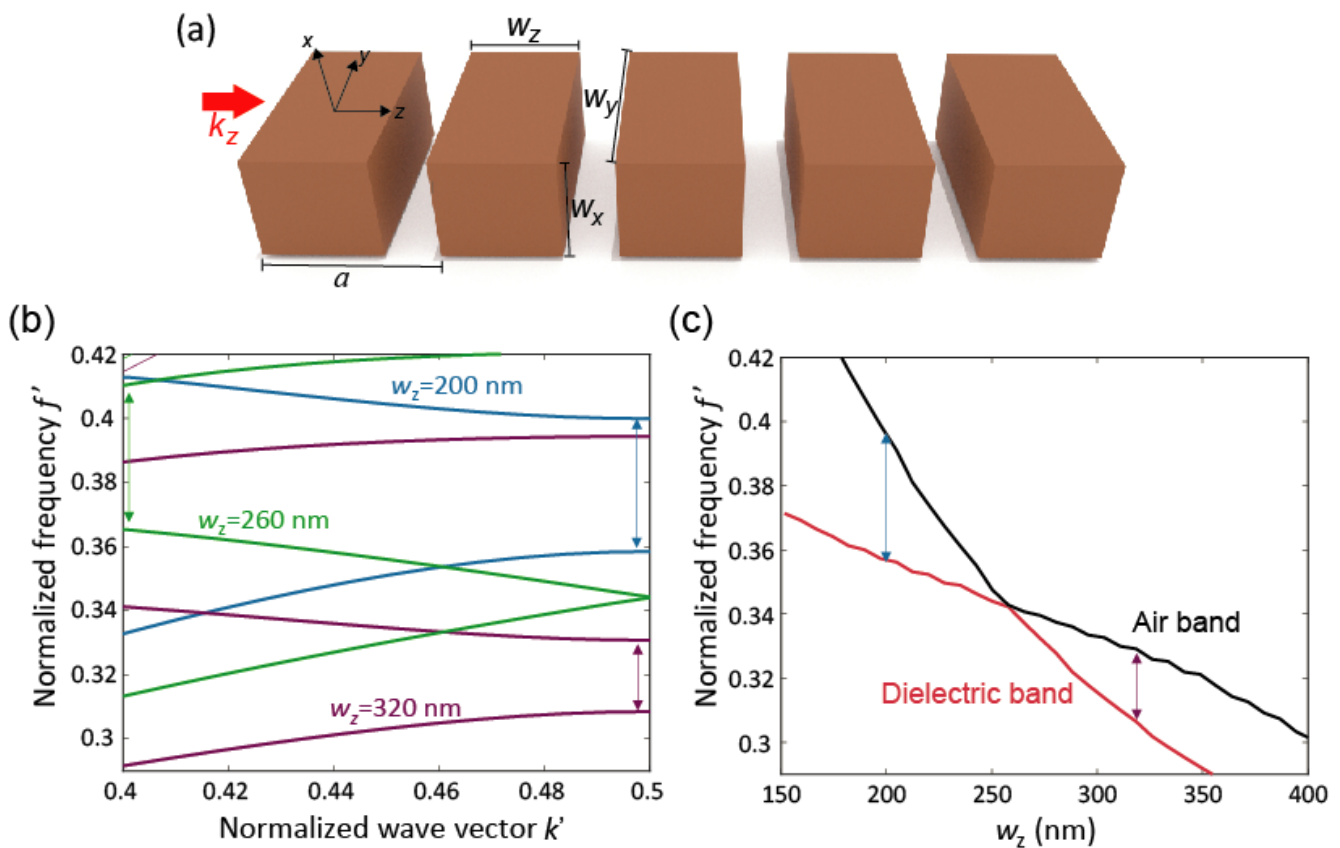
Figure 1. (**a**) Sketch of the 1D periodic systems under study: a chain of high-index dielectric nanobricks. (**b**) Photonic bands for *x*-even parity (TE-like) modes for different values of w_z. (**c**) Frequencies of the dielectric and air bands as a function of w_z. Vertical arrows show the PBG for each value of w_z (for w_z = 260 nm a higher-order PBG is shown). The numerical simulations were performed for a 1D periodic chain of nanobricks with index n = 3.5 and dimensions w_x = 220 nm, w_y = 450 nm, a = 455 nm. The normalized frequency f' is given in units of $\omega a/2\pi c$, ω being the angular frequency and c the speed of light in vacuum. The normalized wave vector k' is given in units of $2\pi k/a$.

We also tested the vanishing behaviour of the PBG using fully 3D finite-difference time-domain (FDTD) simulations. The normalized intensity (square of the electric field at the center of the waveguide) after transmission along a chain of 10 nanobricks using rectangular waveguides of width w_x and thickness w_y for different values of w_z is shown in Figure 2. Normalization is performed with respect to the response of a single waveguide. Notice that intensities over 1 (0 dB) are because the electric field is monitored locally, so resonant effects (such as Fabry–Perot fringes close to the PBG regions) can lead to large local intensities, though the normalized transmitted power is always lower than 1. In agreement with Figure 1b, whilst broad dips appear for w_z = 200 nm and w_z = 320 nm at the expected frequency bands, there is not any observable dip for w_z = 260 nm (the fall in transmission above f' = 0.37 corresponds to higher-order PBGs, as shown in Figure 1b).

To obtain further insights about the closure of the Bragg PBG, we obtained the main components of the transverse electric field at k' = 0.5 for the dielectric and air bands at different values of w_z. The results are illustrated in Figure 3. For w_z = 200 nm, the dielectric band is characterized by a *z*-even parity transverse electric field (E_y) closely resembling an electric dipole pointing along *y*. The air band shows an opposite behavior in terms of parity, and the electric field patterns corresponds to those of a magnetic dipole oriented along *x* (the magnetic field pattern is not shown here for the sake of simplicity). For w_z = 320 nm, the situation completely reverses; now, the dielectric (air) band has a magnetic (electric) dipole character. Therefore, it is the transition from electric to magnetic Mie resonances of

the isolated nanobricks that explains the closure of the Bragg PBG. Indeed, the bandgap is closed because, for certain dimensions of the system, the Mie electric and magnetic resonances of the isolated nanobrick become degenerate at a frequency within a Bragg PBG. The band flip can also be observed in the Supplementary Visualizations 1 to 12, which show the evolution of the E_y and H_x fields when propagating along a chain of ten nanobricks at frequencies corresponding to the dielectric band, the bandgap and the air band and for $w_z = 200$ and 320 nm, respectively.
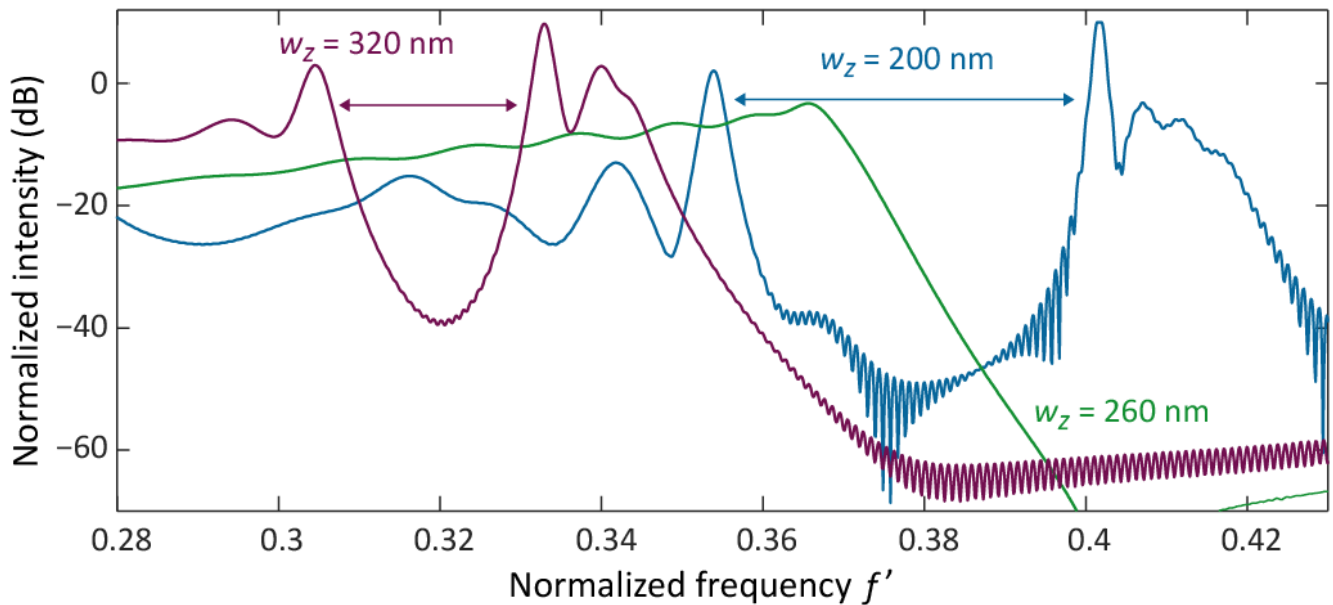

Figure 2. FDTD-calculated normalized intensity after transmission along a chain of 10 nanobricks using waveguides as input and output ports for $w_z = 200$ (blue), 260 (black) and 320 nm (red). The results are normalized with respect to the transmission along a perfect rectangular waveguide. The trend is as follows: the PBG (highlighted by the horizontal lines with arrows) shifts to lower frequencies when w_z increases and disappears at $w_z \approx 260$ nm.
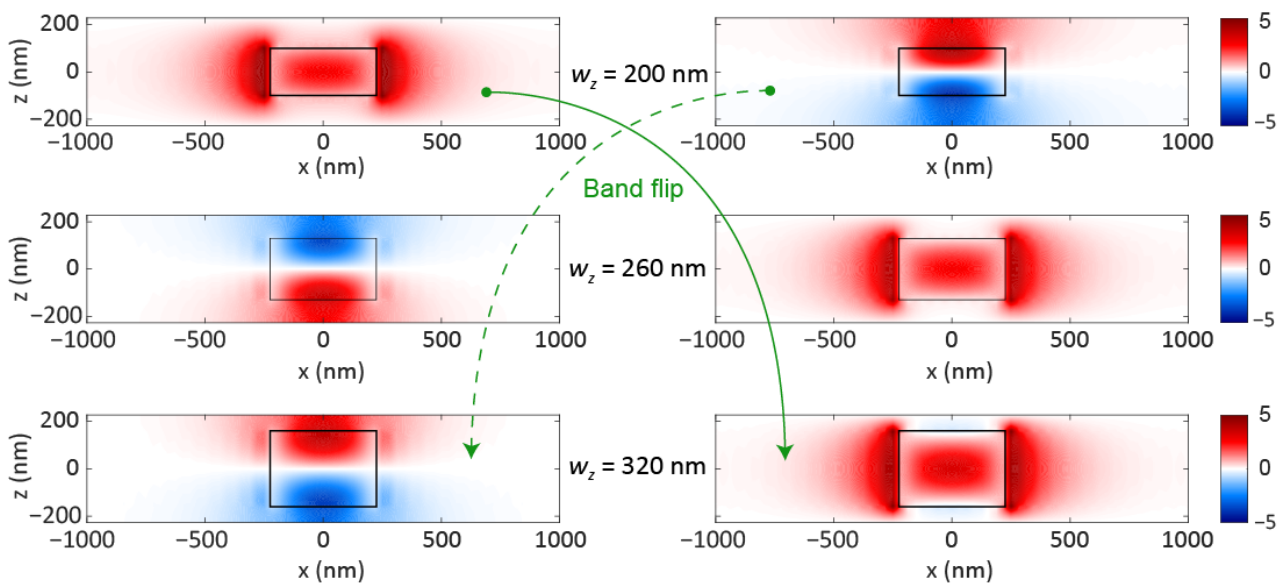
Figure 3. E_y field maps at the boundary of the first Brillouin zone for the dielectric (left column) and air (right column) bands at different values of w_z. For $w_z = 260$ nm (middle panels) the frequency difference between the two bands is negligible, meaning that they are close to the degeneracy point.

To support this explanation, we calculated the frequencies of the electric and magnetic dipole responses of isolated nanobricks as a function of w_z, following the approach in [13]. The results, depicted in Figure 4, show that, for small values of w_z, the frequency of the electric dipole is smaller than that of the magnetic dipole, and this feature is inherited by the dielectric and air bands when the periodic system is formed. When w_z increases, the frequency of the magnetic dipole decreases faster than that of the electric dipole, resulting in the crossing of the Mie resonances, which are related to the band flipping and PBG closure in the periodic system. Indeed, even though we have only studied the effects of the w_z variation for simplicity, we can state that, for a given target frequency, there will be a triplet of (w_x, w_y, w_z) values for which the electric and magnetic dipole resonances are degenerate. Therefore, it will be always possible to design a 1D periodic system with a closed bandgap at a certain wavelength. Moreover, if the degeneracy is achieved for a nanobrick with $w_x = w_y$, the Bragg PBG will be closed for both TE and TM modes simultaneously as a result of the symmetry of the system.
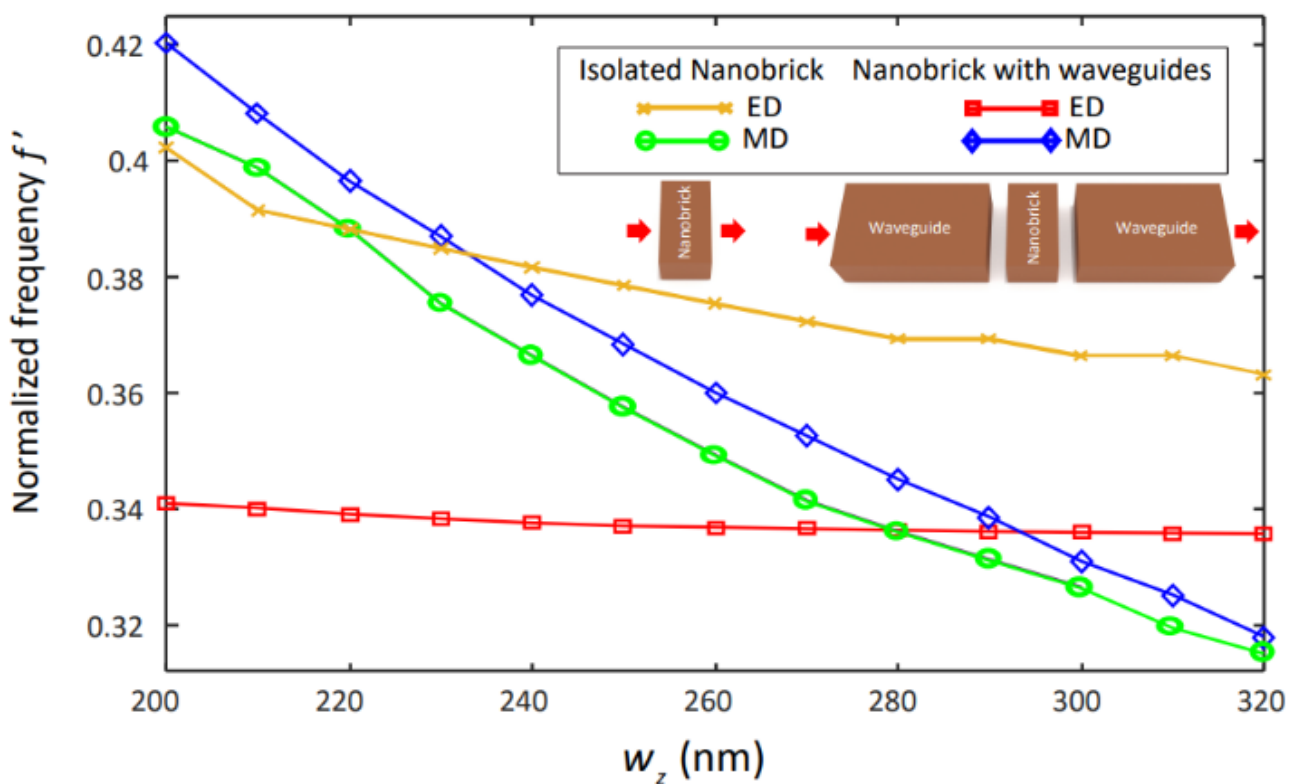
Figure 4. Calculation of the electric (orange) and magnetic (green) dipole frequencies of an isolated nanobrick as a function of w_z obtained from a multipole decomposition. The red and blue curves show the frequencies of the maximum E_y and H_x at the nanobrick center when the nanobrick is embedded in a waveguide gap (illumination and collection using the TE-like mode of the waveguide ports). Inset: scheme of the illumination of the silicon nanobrick for each result.

Notice that the crossing of the electric and magnetic dipole of the isolated nanobricks takes place for a w_z value smaller than that obtained for the PBG closure. However, this can be explained because the isolated nanobrick is surrounded by a vacuum; when forming the chain part of the field, the electromagentic field penetrates the neighbouring nanobricks, resulting in a perturbation of the modes. To account for the additional presence of dielectric material, we calculated the frequencies of the electric and magnetic dipoles corresponding to the maximum of the electric field and the magnetic field at the center of the nanobrick, respectively; this occurred when a single nanobrick was embedded in a waveguide gap of a length equal to *a* (see Figure 4, inset). The results, also shown in Figure 4, indicate that, now, the flip frequency is red-shifted and the crossing point shifts to larger values of w_z.

3. Discussion and Conclusions

Our results highlight the importance of the properties of the isolated unit cell when forming 1D lattices of high-index dielectric materials [14]. Noticeably, when the Mie resonances of the unit cell dominate over the periodic response, the structure could, in principle, be considered as an all-dielectric metamaterial [15]. However, looking at the classification proposed in [16], the PBG closure takes place just when the Bragg wavelength equals the electric and magnetic dipole wavelengths, meaning that we are just at the frontier separating the photonic crystal and metamaterial phases. Indeed, in the 2D periodic systems arranged in a square lattice studied in [16], which require very large indices to reach the metamaterial phase, the use of a hexagonal lattice [17] would allow one to obtain a "metamaterial" behavior in 2D silicon photonic crystals. Our results show that such metamaterial behavior naturally arises in a realistic 1D photonic crystal made of silicon nanobricks at bands placed below the light cone, which would ensure lossless performance. This behavior is manifested by the fact that the overlapping of the electric and magnetic dipolar Mie resonances closes the Bragg PBG, which is the fundamental feature of a photonic crystal.

In summary, we have shown that the interplay between the electric and magnetic dipole resonances of a single nanobrick can lead to the closure of the Bragg PBG for guided modes when forming a 1D photonic crystal. This result is somewhat counterintuitive since, in principle, any 1D periodic lattice should induce a forbidden band for waves propagating in the direction of the periodicity. Even though we have analyzed a very simple structure, the performance should be the same if the unit cell supports electric and magnetic resonances so that a band flip might arise under certain conditions. Noticeably, the PBG only vanishes for a perfect photonic crystal, so any tiny perturbation can open the PBG. This could be used to build active or tunable devices where the properties of a single nanobrick can be actively modified using electrical, optical or even mechanical means. Our finding could lead to advances in the design of subwavelength integrated photonic devices [18] for application in signal processing, communication systems or bio- and chemo-sensing. Notably, the resulting devices could be easily manufactured using mainstream silicon photonic technology.

References

1. Joannopoulos, J.D.; Villeneuve, P.R.; Fan, S. Photonic crystals: Putting a new twist on light. *Nature* **1997**, *386*, 143–149. [CrossRef]
2. Oh, M.C.; Lee, H.J.; Lee, M.H.; Ahn, J.H.; Han, S.G.; Kim, H.G. Tunable wavelength filters with Bragg grating fiber in polymer waveguides. *Appl. Phys. Lett.* **1998**, *73*, 2543–2545. [CrossRef]

3.   Ho, K.M.; Chan, C.T.; Soukoulis, C.M. Existence of a photonic gap in periodic dielectric structures. *Phys. Rev. Lett.* **1990**, *65*, 3152–3155. [CrossRef] [PubMed]

4.   Blanco, A.; Chomski, E.; Grabtchak, S.; Ibisate, M.; Jhon, S.; Leonard, S.W.; Lopez, C.; Meseguer, F.; Miguez, H.; Mondia, J.P.; et al. Large-scale synthesis of a silicon photonic crystal with a complete three-dimensional bandgap near 1.5 micrometres. *Nature* **2000**, *405*, 437–440. [CrossRef] [PubMed]

5.   Martínez, A.; García, J.; Sanchis, P.; Cuesta-Soto, F.; Blasco, J.; Martí, J. Intrinsic losses of coupled-cavity waveguides in planar-photonic crystals. *Opt. Lett.* **2007**, *32*, 635–637. [CrossRef]

6.   Halir, R.; Bock, P.J.; Cheben, P.; Ortega-Moñux, A.; Alonso-Ramos, C.; Schmid, J.H.; Lapointe, J.; Xu, D.; Wangüemert-Pérez, J.G.; Molina-Fernández, Í.; et al. Waveguide sub-wavelength structures: A review of principles and applications. *Laser Photonics Rev.* **2015**, *9*, 25–49. [CrossRef]

7.   Lee, S.G.; Magnusson, R. Essential differences between TE and TM band gaps in periodic films at the first Bragg condition. *Opt. Lett.* **2019**, *44*, 4658–4661. [CrossRef] [PubMed]

8.   García, J.; Sanchis, P.; Martínez, A.; Martí, J. 1D periodic structures for slow-wave induced non-linearity enhancement. *Opt. Express* **2008**, *16*, 3146–3160. [CrossRef] [PubMed]

9.   Ding, L.; Morits, D.; Bakker, R.; Li, S.; Eschimese, D.; Zhu, S.; Yu, Y.F.; Paniagua-Dominguez, R.; Kuznetsov, A.I. All-Optical Modulation in Chains of Silicon Nanoantennas. *ACS Photonics* **2020**, *7*, 1001–1008. [CrossRef]

10.   Pereira-Martín, D.; Luque-González, J.M.; Wangüemert-Pérez, J.G.; Hadij-ElHouati, A.; Molina-Fernández, Í.; Cheben, P.; Schmid, J.H.; Wang, S.; Ye, W.N.; Čtyroký, J.; et al. Complex spectral filters in silicon waveguides based on cladding-modulated Bragg gratings. *Opt. Express* **2021**, *29*, 15867–15881. [CrossRef] [PubMed]

11.   Farnesi, D.; Pelli, S.; Soria, S.; Conti, G.N.; Le Roux, X.; Ballester, M.M.; Vivien, L.; Cheben, P.; Ramos, C.A. Metamaterial engineered silicon photonic coupler for whispering gallery mode microsphere and disk resonators. *Optica* **2021**, *8*, 1511–1514. [CrossRef]

12.   Espinosa-Soria, A.; Martínez, A. Transverse spin and spin-orbit coupling in silicon waveguides. *IEEE Photonics Technol. Lett.* **2016**, *28*, 1561–1564. [CrossRef]

13.   Díaz-Escobar, E.; Bauer, T.; Pinilla-Cienfuegos, E.; Barreda, A.I.; Griol, A.; Kuipers, L.; Martínez, A. Radiationless anapole states in on-chip photonics. *Light. Sci. Appl.* **2021**, *10*, 204. [CrossRef]

14.   Kuznetsov, A.I.; Miroshnichenko, A.E.; Brongersma, M.L.; Kivshar, Y.S.; Luk'yanchuk, B. Optically resonant dielectric nanostructures. *Science* **2016**, *354*, 2472. [CrossRef] [PubMed]

15.   Staude, I.; Schilling, J. Metamaterial-inspired silicon nanophotonics. *Nat. Photonics* **2017**, *11*, 274–284. [CrossRef]

16.   Rybin, M.V.; Filonov, D.; Samusev, K.B.; Belov, P.A.; Kivshar, Y.S.; Limonov, M.F. Phase diagram for the transition from photonic crystals to dielectric metamaterials. *Nat. Commun.* **2015**, *6*, 10102. [CrossRef] [PubMed]

17.   Li, S.V.; Kivshar, Y.S.; Rybin, M.V. Toward Silicon-Based Metamaterials. *ACS Photonics* **2018**, *5*, 4751–4757. [CrossRef]

18.   Cheben, P.; Halir, R.; Schmid, J.H.; Atwater, H.A.; Smith, D.R. Subwavelength integrated photonics. *Nature* **2018**, *560*, 565–572. [CrossRef] [PubMed]